Aust. J. Phys., 1984, **37**, 475–86

L-subshell X-ray Production by 100–250 keV/a.m.u. Ions

M. F. Harrigan,[A] *B. M. Spicer*[A] *and D. D. Cohen*[B]

[A] School of Physics, University of Melbourne, Parkville, Vic. 3052.
[B] Australian Institute of Nuclear Science and Engineering, Private Mail Bag, Sutherland, N.S.W. 2232.

Abstract

Individual L-subshell ionization cross sections have been measured for bombardment of 100–200 keV H^+ ions in 10 keV steps upon a thick Gd ($Z = 64$) target and for bombardment of 600–1000 keV He^+ ions in 100 keV steps upon thick W ($Z = 74$) and thick and thin Au ($Z = 79$) targets. Experimental results for the individual L subshells are compared with the theoretical predictions of the ECPSSR theory as developed by Brandt and Lapicki. The differences are discussed as a function of the reduced ion velocity. The occurrence of collision induced intra-shell transitions is discussed as a possible source for the discrepancy between experiment and theory.

1. Introduction

The theory of inner shell ionization by ion bombardment, as developed by Brandt and his coworkers over the past decade culminating in the ECPSSR theory (Brandt and Lapicki 1979, 1981), describes the ionization process in terms of a projectile perturbed by the Coulomb field (C) of the nucleus and the target electron orbits in terms of screened hydrogenic (SCH) wavefunctions under the influence of the projectile as perturbed stationary states (PSS) with relativistic effects (R). The energy loss (E) of the projectile is incorporated in the Coulomb field and also as a simple multiplicative factor except when exact limits of momentum and energy transfer are used. This so-called ECPSSR theory is incorporated in the plane wave Born approximation (PWBA) formalism as a series of modifications to the effective binding energy and effective projectile energy which appear in the limits of momentum and energy transfer. The ECPSSR theoretical calculations presented here use the exact limits of momentum and energy transfer (for details see the Appendix).

Concurrent with this development has been a renewed interest in ion induced X-ray spectra (as a means of trace elemental analysis) due to improved X-ray detection technology. The publishing by Krause (1979) of a least-squares fit to all current experimental data for K- and L-shell fluorescence yields and Coster–Kronig transition probabilities for elements $5 \leqslant Z \leqslant 110$ has enabled a consistent comparison of both K- and L-shell X-ray production cross sections with the theoretical predictions of the ECPSSR theory.

2. Procedure

The experimental arrangement for He^+ ion bombardment is essentially identical to that described elsewhere (Cohen 1980*a*, 1981*a*). The Australian Atomic Energy

0004-9506/84/050475$02.00

Commission's 3 MV Van de Graaff accelerator was used to bombard a thick tungsten and one thick and (three) thin or transmission gold samples (mounted at 90° to the incident beam direction) with He^+ ions of 600–1000 keV in 100 keV steps. The three transmission Au targets of thickness 375, 222 and 93·8 $\mu g\,cm^{-2}$ were prepared by vacuum evaporation onto polished carbon discs. The range of a 600 keV He^+ ion in Au is 2·22 $mg\,cm^{-2}$. For a 222 $\mu g\,cm^{-2}$ Au target there is an energy loss of ~80 keV for a 600 keV He^+ ion. The 375 and 93·8 $\mu g\,cm^{-2}$ targets were thus used only to check that the 222 $\mu g\,cm^{-2}$ target could be used as a transmission target since, to maximize the yield, the thickest transmission target is required. The transmission target thicknesses were determined and monitored during the data acquisition using Rutherford backscattering at 135°.

The L X-rays produced from He^+ bombardment were detected by an ORTEC 7900T-449 Si(Li) detector with an active area of 12 mm^2 and with an energy resolution of 140 eV at 5·89 keV. The detector was coupled to the vacuum system of the target chamber at 135° to the incident beam direction.

A KAMAN A-1254 neutron generator with a H_2 gas supply was used to produce the 100–200 keV H^+ ions. The beam was mass analysed to remove any H_2^+ contaminants. The beam energy was calibrated using the $^{11}B(p, \gamma)^{12}C$ resonance at 163 keV which was measured at 163·5±1 keV. A thick Gd target mounted at 45° to the incident beam direction was then bombarded with 100–200 keV H^+ ions in 10 keV steps.

The L X-rays produced from H^+ bombardment were detected by an ORTEC SLP-06165 Si(Li) detector with an active area of 28 mm^2 and with an energy resolution of 175 eV at 5·89 keV. The detector was mounted outside the target chamber at 90° to the incident beam direction.

3. Analysis

The absolute efficiencies of the two detectors used were determined using a standard ^{241}Am source and fitted to a function of the form (Cohen 1980*b*)

$$\varepsilon = f_{\mathrm{Be}} f_{\mathrm{Si}} f_{\mathrm{Au}} f_{\mathrm{fil}} f_{\mathrm{g}}(1 - f_{\mathrm{cr}}),$$

where $f_{\mathrm{Be}}, f_{\mathrm{Si}}, f_{\mathrm{Au}}$ and f_{fil} are the X-ray transmission probabilities through the beryllium window, silicon dead layer, gold contact electrode, and any filters present; f_{g} is a geometric factor correcting for losses due to apertures or annular dead layers within the crystal and f_{cr} is the probability of an X-ray escaping the crystal. For the X-ray energy range of interest here (5–20 keV) the detection efficiency, including filter effects, was always better than 50%.

Each spectrum was fitted using standard gaussian peak shapes upon a scaled linear background. The raw peak areas obtained were corrected for total detection efficiency and divided by the deadtime corrected total charge to obtain a yield in counts per μC per 100% efficiency for each of the L X-ray transitions of interest ($L_l, L_\alpha, L_\beta, L_\gamma, L_{\gamma_1}, L_{\mathrm{tot}}$) over the whole range of bombarding energies. The yields obtained were fitted to an empirical function of the form

$$I_p(E) = a(E/b - 1)^c,$$

where a, b and c are the least-squares fitted constants for a given transition p and $I_p(E)$ is the yield in counts per μC per 100% efficiency at bombarding energy E.

For thin (i.e. transmission) targets the X-ray production cross section is related to the raw X-ray yield $Y(E)$ at bombarding energy E by (Cohen 1980*a*)

$$\sigma^{\mathrm{X}}(E) = 4\pi Y(E)/BN\Omega\varepsilon,$$

where B is the number of atoms per cm^2 in the target, N is the total number of ions hitting the target, Ω is the solid angle in steradians subtended by the ion beam spot at the detector and ε is the total detection efficiency. For singly charged ions traversing a target of thickness X (μm) the X-ray production cross section becomes (in barns)

$$\sigma^{\mathrm{X}}(E) = 2{\cdot}013\times 10^{16}\, Y(E)/AXQ\Omega\varepsilon,$$

where Q is the total charge hitting the target (μC) and A is the number of atoms per cm^3 in the target.

Even for a transmission target the ion will still experience some energy loss ΔE in traversing the target and similarly the emergent X-ray, emitted at an angle θ_0 to the target surface normal, will suffer some attenuation due to self-absorption. This projectile energy loss and X-ray absorption can be allowed for by assuming that all X-rays are produced in the centre of the target.* Hence the X-ray production cross section $\sigma_p^{\mathrm{X}}(E)$ for a peak p at bombarding energy E is related to the corrected yield $I_p(E)$ by

$$\sigma_p^{\mathrm{X}}(E-\tfrac{1}{2}\Delta E) = 2{\cdot}013\times 10^{16} I_p(E-\tfrac{1}{2}\Delta E)/A\Omega X \exp(-0{\cdot}5\mu_p t\sec\theta_0),$$

where μ_p is the X-ray mass attenuation coefficient in cm^2 g^{-1} for an X-ray peak p (Mayer and Rimini 1977) and t is the target thickness in g cm^{-2}.

For thick (i.e. stopping) targets, corrections for the projectile energy loss and X-ray attenuation require more rigorous treatment. Merzbacher and Lewis (1958) derived a simple expression relating the X-ray production cross section to the X-ray yield from a thick target that depends upon the change in yield with energy which, when related to the corrected yield $I_p(E)$, becomes

$$\sigma_p^{\mathrm{X}}(E) = \frac{2{\cdot}013\times 10^{12}\rho}{A\Omega}\left(S(E)\frac{\mathrm{d}I_p(E)}{\mathrm{d}E} + \mu_p\frac{\cos\theta_{\mathrm{i}}}{\cos\theta_0} I_p(E)\right),$$

where ρ is the target density in g cm^{-3}, $S(E)$ is the stopping power at energy E (MeV cm^2 g^{-1}) (Andersen and Ziegler 1977) and θ_{i} is the ion inward angle relative to the target normal.

The fitting of the yield in counts per μC per 100% efficiency in the form $a(E/b-1)^c$ allows the change in yield as a function of ion energy $[\mathrm{d}I_p(E)/\mathrm{d}E]$ to be easily determined for the thick target relationship. The experimentally determined individual L-shell ionization cross sections (σ_i^{I}, $i = 1, 2, 3$) were then determined by unfolding the relationship between σ_p^{X} and σ_i^{I} using the (a) α, β, γ lines and (b) $\alpha, \gamma_1, L_{\mathrm{tot}}(\bar{\omega})$ transitions (as outlined previously by Cohen 1980*a*, 1981*a*) and taking the mean of the two results. The fluorescence yields and Coster–Kronig transition probabilities of Krause (1979), together with the emission rates of Salem *et al.* (1974), were used throughout.

* Note that for a thin target this will correspond to the point where the bombarding ion has energy $E-\tfrac{1}{2}\Delta E$.

Table 1. Thick W (Z = 74) ionization cross sections

He$^+$ energy (MeV)	Reduced velocity	σ_{exp} (b)	σ_{theory} (b)	$\sigma_{exp}/\sigma_{theory}$
		L_{tot} shell		
0·6	0·2300	$8\cdot31\times10^{-2}$	$5\cdot93\times10^{-2}$	1·40
0·7	0·2468	$2\cdot38\times10^{-1}$	$1\cdot56\times10^{-1}$	1·52
0·8	0·2624	$5\cdot19\times10^{-1}$	$3\cdot34\times10^{-1}$	1·55
0·9	0·2771	$9\cdot63\times10^{-1}$	$6\cdot17\times10^{-1}$	1·56
1·0	0·2910	1·61	1·03	1·56
				Mean: 1·52
				s.d.: 0·07
		L_3 subshell		
0·6	0·2300	$3\cdot53\times10^{-2}$	$2\cdot60\times10^{-2}$	1·35
0·7	0·2468	$1\cdot05\times10^{-1}$	$7\cdot17\times10^{-2}$	1·46
0·8	0·2624	$2\cdot45\times10^{-1}$	$1\cdot60\times10^{-1}$	1·53
0·9	0·2771	$4\cdot88\times10^{-1}$	$3\cdot08\times10^{-1}$	1·58
1·0	0·2910	$8\cdot67\times10^{-1}$	$5\cdot35\times10^{-1}$	1·62
				Mean: 1·51
				s.d.: 0·11
		L_2 subshell		
0·6	0·2076	$1\cdot68\times10^{-2}$	$3\cdot80\times10^{-3}$	4·43
0·7	0·2226	$4\cdot64\times10^{-2}$	$1\cdot12\times10^{-2}$	4·16
0·8	0·2365	$9\cdot98\times10^{-2}$	$2\cdot61\times10^{-2}$	3·82
0·9	0·2495	$1\cdot82\times10^{-1}$	$5\cdot24\times10^{-2}$	3·48
1·0	0·2619	$2\cdot97\times10^{-1}$	$9\cdot39\times10^{-2}$	3·16
				Mean: 3·81
				s.d.: 0·51
		L_1 subshell		
0·6	0·2080	$3\cdot05\times10^{-2}$	$2\cdot95\times10^{-2}$	1·03
0·7	0·2224	$8\cdot57\times10^{-2}$	$7\cdot35\times10^{-2}$	1·17
0·8	0·2358	$1\cdot72\times10^{-1}$	$1\cdot48\times10^{-1}$	1·17
0·9	0·2484	$2\cdot91\times10^{-1}$	$2\cdot57\times10^{-1}$	1·13
1·0	0·2604	$4\cdot24\times10^{-1}$	$4\cdot03\times10^{-1}$	1·10
				Mean: 1·12
				s.d.: 0·06

4. Results and Discussion

Tables 1 and 2 show the individual and total L-shell ionization cross sections obtained for thick W (Z = 74) and thick Gd (Z = 64). The results from both thick and thin Au (Z = 79) are shown in Table 3. The systematic differences between the thin and thick target results are usually within experimental uncertainties except for the L_1 subshell which is essentially obtained by the subtraction of two large but approximately equal numbers. The mean of the two results is taken in order to minimize any systematic errors that may have occurred due to experimental peak fitting inaccuracies. In order to compare the data obtained with that taken previously (Cohen 1981*a*, 1981*b*), a mean value over the range of the reduced velocity of the bombarding ion used is also given. The reduced velocity of the bombarding ion is just the ratio of the target electron orbital time (corrected for relativistic and binding effects) to the collision time (corrected for energy loss and Coulomb deflection).

Table 2. Thick Gd ($Z = 64$) ionization cross sections

H^+ energy (MeV)	Reduced velocity	σ_{exp} (b)	σ_{theory} (b)	$\sigma_{exp}/\sigma_{theory}$	H^+ energy (MeV)	Reduced velocity	σ_{exp} (b)	σ_{theory} (b)	$\sigma_{exp}/\sigma_{theory}$
		L_{tot} shell					L_2 subshell		
0·10	0·2278	$1{\cdot}44\times10^{-3}$	$1{\cdot}66\times10^{-3}$	0·87	0·10	0·2103	$3{\cdot}13\times10^{-4}$	$1{\cdot}25\times10^{-4}$	2·50
0·11	0·2382	$4{\cdot}53\times10^{-3}$	$4{\cdot}57\times10^{-3}$	0·99	0·11	0·2198	$8{\cdot}86\times10^{-4}$	$3{\cdot}67\times10^{-4}$	2·42
0·12	0·2481	$1{\cdot}14\times10^{-2}$	$1{\cdot}05\times10^{-2}$	1·08	0·12	0·2288	$2{\cdot}09\times10^{-3}$	$8{\cdot}99\times10^{-4}$	2·32
0·13	0·2576	$2{\cdot}46\times10^{-2}$	$2{\cdot}15\times10^{-2}$	1·14	0·13	0·2376	$4{\cdot}35\times10^{-3}$	$1{\cdot}93\times10^{-3}$	2·25
0·14	0·2668	$4{\cdot}77\times10^{-2}$	$3{\cdot}95\times10^{-2}$	1·21	0·14	0·2460	$8{\cdot}25\times10^{-3}$	$3{\cdot}73\times10^{-3}$	2·21
0·15	0·2756	$8{\cdot}49\times10^{-2}$	$6{\cdot}69\times10^{-2}$	1·27	0·15	0·2540	$1{\cdot}45\times10^{-2}$	$6{\cdot}61\times10^{-3}$	2·19
0·16	0·2842	$1{\cdot}42\times10^{-1}$	$1{\cdot}07\times10^{-1}$	1·33	0·16	0·2619	$2{\cdot}42\times10^{-2}$	$1{\cdot}10\times10^{-2}$	2·20
0·17	0·2925	$2{\cdot}24\times10^{-1}$	$1{\cdot}62\times10^{-1}$	1·39	0·17	0·2695	$3{\cdot}84\times10^{-2}$	$1{\cdot}73\times10^{-2}$	2·22
0·18	0·3005	$3{\cdot}41\times10^{-1}$	$2{\cdot}34\times10^{-1}$	1·46	0·18	0·2769	$5{\cdot}84\times10^{-2}$	$2{\cdot}60\times10^{-2}$	2·25
0·19	0·3084	$4{\cdot}99\times10^{-1}$	$3{\cdot}27\times10^{-1}$	1·52	0·19	0·2841	$8{\cdot}61\times10^{-2}$	$3{\cdot}76\times10^{-2}$	2·29
0·20	0·3160	$7{\cdot}08\times10^{-1}$	$4{\cdot}44\times10^{-1}$	1·59	0·20	0·2911	$1{\cdot}23\times10^{-1}$	$5{\cdot}27\times10^{-2}$	2·34
				Mean: 1·26					Mean: 2·29
				s.d.: 0·23					s.d.: 0·10
		L_3 subshell					L_1 subshell		
0·10	0·2278	$6{\cdot}99\times10^{-4}$	$8{\cdot}41\times10^{-4}$	0·83	0·10	0·2063	$4{\cdot}30\times10^{-4}$	$6{\cdot}96\times10^{-4}$	0·62
0·11	0·2382	$2{\cdot}19\times10^{-3}$	$2{\cdot}30\times10^{-3}$	0·95	0·11	0·2153	$1{\cdot}46\times10^{-3}$	$1{\cdot}89\times10^{-3}$	0·77
0·12	0·2481	$5{\cdot}48\times10^{-3}$	$5{\cdot}34\times10^{-3}$	1·03	0·12	0·2240	$3{\cdot}82\times10^{-3}$	$4{\cdot}30\times10^{-3}$	0·89
0·13	0·2576	$1{\cdot}18\times10^{-2}$	$1{\cdot}10\times10^{-2}$	1·08	0·13	0·2324	$8{\cdot}45\times10^{-3}$	$8{\cdot}59\times10^{-3}$	0·98
0·14	0·2668	$2{\cdot}28\times10^{-2}$	$2{\cdot}03\times10^{-2}$	1·12	0·14	0·2404	$1{\cdot}66\times10^{-2}$	$1{\cdot}54\times10^{-2}$	1·08
0·15	0·2756	$4{\cdot}07\times10^{-2}$	$3{\cdot}49\times10^{-2}$	1·17	0·15	0·2480	$2{\cdot}97\times10^{-2}$	$2{\cdot}54\times10^{-2}$	1·17
0·16	0·2842	$6{\cdot}78\times10^{-2}$	$5{\cdot}64\times10^{-2}$	1·20	0·16	0·2556	$4{\cdot}98\times10^{-2}$	$3{\cdot}94\times10^{-2}$	1·26
0·17	0·2925	$1{\cdot}07\times10^{-1}$	$8{\cdot}64\times10^{-2}$	1·24	0·17	0·2628	$7{\cdot}88\times10^{-2}$	$5{\cdot}78\times10^{-2}$	1·36
0·18	0·3005	$1{\cdot}63\times10^{-1}$	$1{\cdot}27\times10^{-1}$	1·29	0·18	0·2699	$1{\cdot}19\times10^{-1}$	$8{\cdot}12\times10^{-2}$	1·47
0·19	0·3084	$2{\cdot}38\times10^{-1}$	$1{\cdot}80\times10^{-1}$	1·32	0·19	0·2767	$1{\cdot}74\times10^{-1}$	$1{\cdot}10\times10^{-1}$	1·58
0·20	0·3160	$3{\cdot}38\times10^{-1}$	$2{\cdot}47\times10^{-1}$	1·37	0·20	0·2834	$2{\cdot}46\times10^{-1}$	$1{\cdot}45\times10^{-1}$	1·70
				Mean: 1·15					Mean: 1·17
				s.d.: 0·16					s.d.: 0·34

Table 3. Au ($Z = 79$) ionization cross sections

He$^+$ energy (MeV)	Reduced velocity	σ_{exp} (b) Thick	σ_{exp} (b) Thin	σ_{exp} (b) Thin–thick	σ_{theory} (b)	$\sigma_{exp}/\sigma_{theory}$ Thick	$\sigma_{exp}/\sigma_{theory}$ Thin	$\sigma_{exp}/\sigma_{theory}$ Thin–thick
				L_{tot} shell				
0·6	0·2173	$2·07\times10^{-2}$	$1·64\times10^{-2}$	$1·86\times10^{-2}$	$1·63\times10^{-2}$	1·27	1·00	1·14
0·7	0·2328	$6·85\times10^{-2}$	$6·09\times10^{-2}$	$6·47\times10^{-2}$	$4·80\times10^{-2}$	1·43	1·27	1·35
0·8	0·2471	$1·65\times10^{-1}$	$1·50\times10^{-1}$	$1·58\times10^{-1}$	$1·11\times10^{-1}$	1·49	1·36	1·43
0·9	0·2607	$3·30\times10^{-1}$	$2·99\times10^{-1}$	$3·15\times10^{-1}$	$2·17\times10^{-1}$	1·52	1·38	1·45
1·0	0·2735	$5·83\times10^{-1}$	$5·24\times10^{-1}$	$5·54\times10^{-1}$	$3·79\times10^{-1}$	1·54	1·38	1·46
						Mean: 1·45	1·28	1·37
						s.d.: 0·11	0·16	0·13
				L_3 subshell				
0·6	0·2173	$8·84\times10^{-3}$	$9·11\times10^{-3}$	$8·97\times10^{-3}$	$7·40\times10^{-3}$	1·19	1·23	1·21
0·7	0·2328	$2·94\times10^{-2}$	$3·02\times10^{-2}$	$2·98\times10^{-2}$	$2·25\times10^{-2}$	1·31	1·34	1·33
0·8	0·2471	$7·13\times10^{-2}$	$7·28\times10^{-2}$	$7·20\times10^{-2}$	$5·36\times10^{-2}$	1·33	1·36	1·34
0·9	0·2607	$1·44\times10^{-1}$	$1·46\times10^{-1}$	$1·45\times10^{-1}$	$1·09\times10^{-1}$	1·32	1·34	1·33
1·0	0·2735	$2·56\times10^{-1}$	$2·59\times10^{-1}$	$2·58\times10^{-1}$	$1·96\times10^{-1}$	1·30	1·32	1·31
						Mean: 1·29	1·32	1·30
						s.d.: 0·06	0·05	0·05
				L_2 subshell				
0·6	0·1936	$3·32\times10^{-3}$	$4·28\times10^{-3}$	$3·80\times10^{-3}$	$8·36\times10^{-4}$	3·97	5·12	4·55
0·7	0·2071	$1·08\times10^{-2}$	$1·28\times10^{-2}$	$1·18\times10^{-2}$	$2·76\times10^{-3}$	3·92	4·64	4·28
0·8	0·2197	$2·61\times10^{-2}$	$2·84\times10^{-2}$	$2·73\times10^{-2}$	$7·00\times10^{-3}$	3·73	4·06	3·90
0·9	0·2316	$5·30\times10^{-2}$	$5·30\times10^{-2}$	$5·30\times10^{-2}$	$1·49\times10^{-2}$	3·55	3·55	3·55
1·0	0·2428	$9·51\times10^{-2}$	$8·90\times10^{-2}$	$9·20\times10^{-2}$	$2·81\times10^{-2}$	3·39	3·17	3·28
						Mean: 3·70	4·11	3·91
						s.d.: 0·25	0·79	0·52
				L_1 subshell				
0·6	0·1960	$8·54\times10^{-3}$	$3·02\times10^{-3}$	$5·79\times10^{-3}$	$8·08\times10^{-3}$	1·06	0·37	0·72
0·7	0·2091	$2·83\times10^{-2}$	$1·78\times10^{-2}$	$2·31\times10^{-2}$	$2·28\times10^{-2}$	1·24	0·78	1·04
0·8	0·2213	$6·76\times10^{-2}$	$4·41\times10^{-2}$	$5·84\times10^{-2}$	$5·00\times10^{-2}$	1·35	0·98	1·17
0·9	0·2327	$1·34\times10^{-1}$	$1·00\times10^{-1}$	$1·17\times10^{-1}$	$9·30\times10^{-2}$	1·44	1·08	1·26
1·0	0·2435	$2·31\times10^{-1}$	$1·76\times10^{-1}$	$2·04\times10^{-1}$	$1·54\times10^{-1}$	1·50	1·14	1·32
						Mean: 1·32	0·87	1·10
						s.d.: 0·17	0·31	0·24

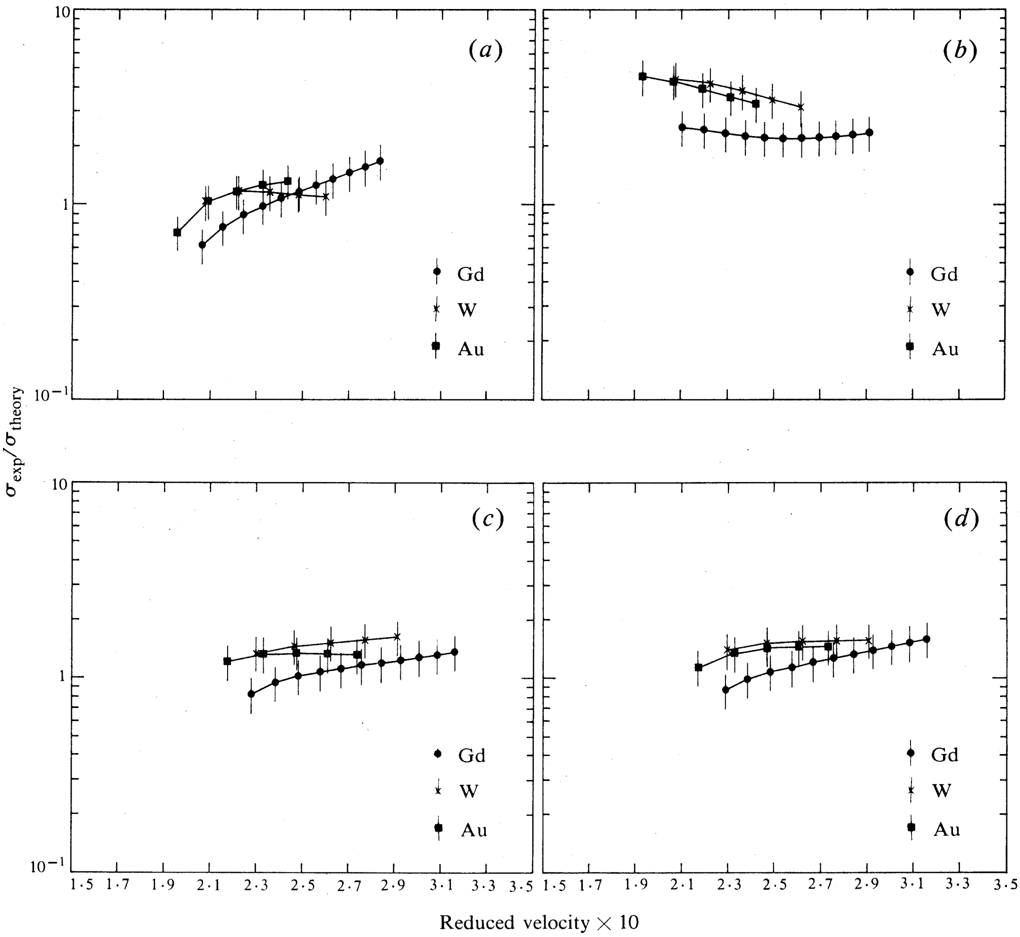

Fig. 1. Plot of the ratio $\sigma_{\rm exp}/\sigma_{\rm theory}$ against reduced ion velocity for Gd, W and Au for the (*a*) L_1 subshell, (*b*) L_2 subshell, (*c*) L_3 subshell, (*d*) $L_{\rm tot}$ shell. The solid curves are not least-squares fits to the data but are inserted for clarity.

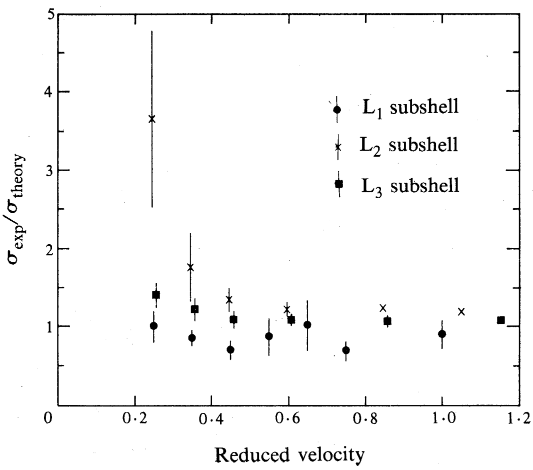

Fig. 2. Plot of the ratio $\sigma_{\rm exp}/\sigma_{\rm theory}$ against reduced ion velocity for current and previous (Cohen 1981*a*, 1981*b*) experimental data. The data are plotted in corrected reduced ion velocity bins. There is an increasing deviation from unity for the L_2 subshell as the reduced ion velocity decreases.

The ratios of $\sigma_{\text{exp}}/\sigma_{\text{theory}}$ obtained (see Fig. 1) exhibit a trend with ion energy consistent with data published previously (Cohen 1981*a*, 1981*b*) taken at higher bombarding energies, indicating an increasing deviation between experiment and theory as the reduced velocity decreases (see Fig. 2).

Because of uncertainties in the atomic parameters, such as fluorescence yields and Coster–Kronig transition probabilities etc., as well as uncertainties in the fits to the absolute yields per μC for the component X-rays (usually better than 5%) and in stopping power data, target thicknesses etc., the absolute cross sections measured are known to within $\pm 21\%$ for the L_{tot} shell and L_3 subshell, $\pm 20\%$ for the L_2 subshell and $\pm 23\%$ for the L_1 subshell.

For W (Table 1), the ECPSSR theoretical cross section underpredicts the experimental values for the L_3 and L_{tot} cross sections with ratios of $\sigma_{\text{exp}}/\sigma_{\text{theory}}$ of $1 \cdot 51 \pm 0 \cdot 11$ and $1 \cdot 52 \pm 0 \cdot 07$ respectively. For the L_1 subshell a smaller deviation is observed with a ratio of $\sigma_{\text{exp}}/\sigma_{\text{theory}} = 1 \cdot 12 \pm 0 \cdot 06$. For the L_2 subshell, however, the ECPSSR theory underpredicts the experimental results by a factor of more than 4 near the lowest bombarding energy with a ratio of $3 \cdot 81 \pm 0 \cdot 51$ over the entire range. Similar deviations for the L_2 shell have been observed for some time for He^+ bombardment of heavy nuclei, although usually for higher bombarding energies ($>1 \cdot 0$ MeV) (Chang *et al.* 1975; Li *et al.* 1976; Sarkadi and Mukoyama 1980).

For Au (Table 3), if we compare the mean of the thick and thin target results, the $\sigma_{\text{exp}}/\sigma_{\text{theory}}$ ratios obtained are similar to those for W for L_3 and L_{tot} ($1 \cdot 30 \pm 0 \cdot 05$ and $1 \cdot 37 \pm 0 \cdot 13$ respectively). For the L_1 subshell the value for $\sigma_{\text{exp}}/\sigma_{\text{theory}}$ of $1 \cdot 10 \pm 0 \cdot 24$ was obtained. For the L_2 subshell the ECPSSR theory again grossly underpredicts the experimental results with a ratio of $3 \cdot 91 \pm 0 \cdot 52$.

For Gd (Table 2), $\sigma_{\text{exp}}/\sigma_{\text{theory}}$ ratios for the L_3 and L_{tot} cross sections are $1 \cdot 15 \pm 0 \cdot 16$ and $1 \cdot 26 \pm 0 \cdot 23$ respectively. For the L_1 subshell of Gd a ratio of $1 \cdot 17 \pm 0 \cdot 34$ was obtained. For the L_2 subshell, however, a much higher ratio was obtained of $2 \cdot 29 \pm 0 \cdot 10$. It should be noted that the results for Gd are from H^+ bombardment and not He^+ as is the case for Au and W. This difference between the ratios obtained suggests an ion-related effect.

The general underprediction of experiment by the ECPSSR theory may, in part, reflect the use of SCH wavefunctions rather than more realistic Dirac–Hartree–Slater (DHS) wavefunctions as suggested by Chen *et al.* (1982) and more recently used in a calculation for K-shell ionization by Mukoyama and Sarkadi (1983). The use of DHS wavefunctions is expected, however, to produce only 10–40% differences in the theoretical predictions of ionization cross sections and hence another mechanism must be sought to explain the current discrepancy. Such a mechanism should possibly include ion effects as well as target effects.

One possible mechanism which could produce the effect is via a collision induced intra-shell transition. Here a primary vacancy initially produced in the L_1 subshell can transfer to the L_2 or L_3 subshell whilst the ionizing projectile is still within the Coulomb field of the nucleus. Transfer to the L_2 subshell is more likely due to the comparatively small difference in binding energy. Such a mechanism is expected to be more significant when the ratio of target electron orbital time to collision time (i.e. the reduced ion velocity) is less than one. For the results reported here the reduced ion velocity ranges from $\sim 0 \cdot 19$ to $\sim 0 \cdot 32$. This mechanism would enhance the experimentally observed L_2 and L_3 subshell ionization cross sections at the expense of the L_1 subshell. This would have a pronounced effect on the experimentally observed ratio of the L_3 ionization cross section to L_2 ionization cross section (see Fig. 3). For a fixed collision velocity such an effect should scale as the Coulomb interaction strength between the ionizing projectile and the target electron (i.e. as the square of the atomic number of the ionizing particle), leading to a higher probability for collision induced transitions for He^+ ions than for H^+ ions.

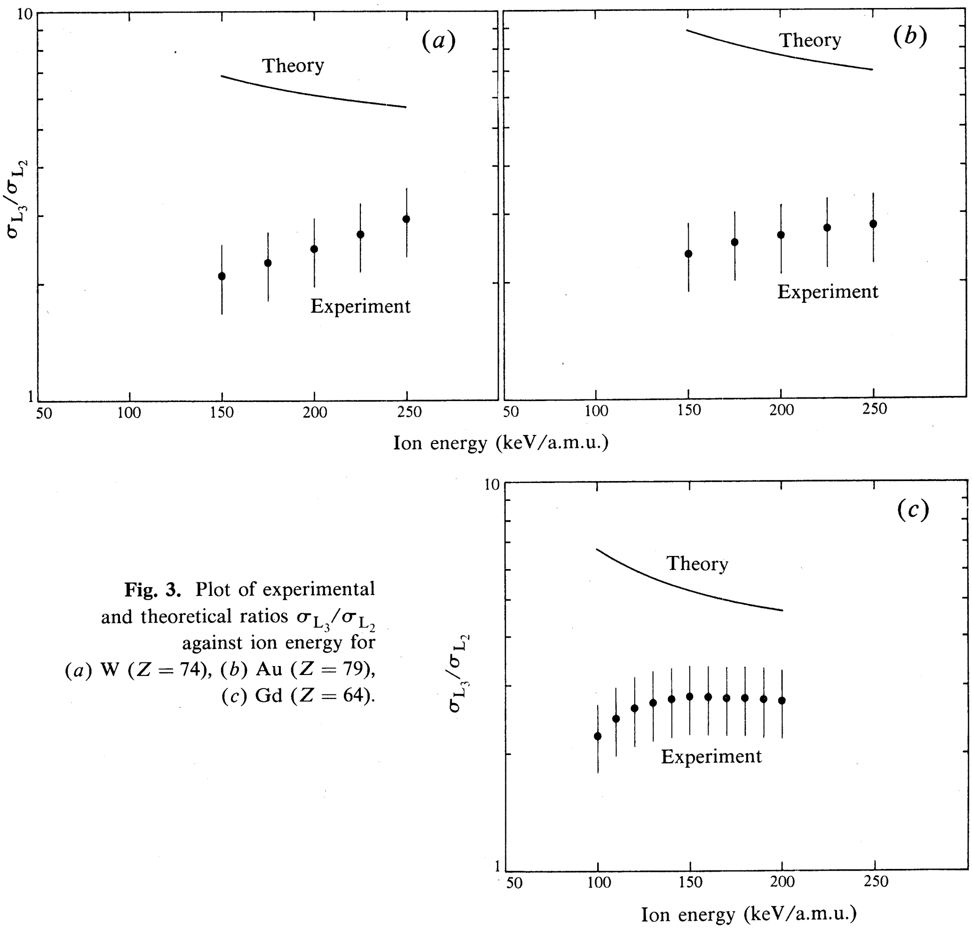

Fig. 3. Plot of experimental and theoretical ratios $\sigma_{L_3}/\sigma_{L_2}$ against ion energy for (*a*) W ($Z = 74$), (*b*) Au ($Z = 79$), (*c*) Gd ($Z = 64$).

Calculations performed by Sarkadi and Mukoyama (1981) and more recently by Finck *et al.* (1983), comparing available experimental data for bombardment of Au by ions ranging from H^+ to ^{16}O, show a pronounced departure from the theoretical predictions of direct ionization cross section theory. They calculated the collision induced intra-shell transition probabilities in a two-step model. Sarkadi and Mukoyama used relativistic Dirac atomic wavefunctions incorporated in the PWBA formalism to obtain RPWBA–BC (binding and Coulomb corrections) calculations for the direct ionization cross sections and a two-step model using the semi-classical approximation (SCA) and retaining only dipole ($\Delta m = 0$) terms for intra-shell transition probabilities. Finck *et al.* calculated the direct ionization cross sections using the CPSSR theory and the intra-shell transition probabilities using the SCA, but retaining both dipole and quadrupole terms. In both cases, although a better agreement between experiment and theory is obtained (especially for bombarding ions which are heavier than He^+), there is still room for substantial improvement in gaining insight into L-shell ionization through the use of higher order ionization theories.

5. Conclusions

Further work is needed in examining the L-shell ionization cross sections for bombarding ions of very low energies ($\leqslant 250$ keV/a.m.u.). In particular, examination of the L_2 subshell should provide a detailed insight into the direct ionization mechanism and collision induced effects through the use of ions of varying atomic number (e.g. H, H_2, He, ...^{16}O). The results reported here suggest that the probability of a collision induced transition for H^+ bombardment is, whilst smaller than that for He^+, not insignificant. The use of DHS wavefunctions incorporated into the ECPSSR theory may provide a more realistic description of the direct ionization process, allowing closer examination of ion-related effects and their scaling with projectile atomic number.

Acknowledgments

The authors acknowledge the assistance of the staff associated with the Australian Atomic Energy Commission's Van de Graaff accelerator. We particularly acknowledge the valuable computer assistance rendered by E. Clayton through the use of his peak-fitting routines. We would also like to acknowledge the financial support of the Australian Institute of Nuclear Science and Engineering. One of us (M.F.H.) also acknowledges the extensive technical support of the Betatron technicians at the University of Melbourne for their assistance with the experimental set-up used for the proton data and the financial support of the Commonwealth Postgraduate Award Scheme.

References

Andersen, H. H., and Ziegler, J. F. (1977). 'Stopping and Ranges of Ions in Matter', Vols 3 and 4 (Pergamon: New York).
Basbas, G., Brandt, W., and Roman, L. (1978). *Phys. Rev.* A **17**, 1655.
Benka, O., and Kropf, A. (1978). *At. Data Nucl. Data Tables* **22**, 219.
Brandt, W., and Lapicki, G. (1979). *Phys. Rev.* A **20**, 465.
Brandt, W., and Lapicki, G. (1981). *Phys. Rev.* A **23**, 1717.
Chang, C. N., Morgan, J. F., and Blatt, S. L. (1975). *Phys. Rev.* A **11**, 1560.
Chen, M. H., Craseman, B., and Mark, H. (1982). *Phys. Rev.* A **26**, 1243.
Cohen, D. D. (1980*a*). *J. Phys.* B **13**, 2953.
Cohen, D. D. (1980*b*). *Nucl. Instrum. Methods* **178**, 481.
Cohen, D. D. (1981*a*). *J. Phys.* B **14**, 2031.
Cohen, D. D. (1981*b*). *Nucl. Instrum. Methods* **191**, 551.
Finck, K., Jitschin, W., and Lutz, H. O. (1983). *J. Phys.* B **17**, L409.
Krause, M. O. (1979). *J. Phys. Chem. Ref. Data* **8**, 307.
Li, T. K., Clark, D. L., and Greenless, G. W. (1976). *Phys. Rev. Lett.* **37**, 1209.
Mayer, J. W., and Rimini, E. (1977). 'Ion Beam Handbook for Material Analysis' (Academic: New York).
Merzbacher, E., and Lewis, H. W. (1958). 'Encyclopedia of Physics', Vol. 34, p. 166 (Springer: Berlin).
Mukoyama, T., and Sarkadi, L. (1983). *Phys. Rev.* A **28**, 1303.

Salem, S. I., Panossian, S. L., and Krause, R. A. (1974). *At. Data Nucl. Data Tables* **14**, 91.
Sarkadi, L., and Mukoyama, T. (1980). *J. Phys.* B **13**, 2255.
Sarkadi, L., and Mukoyama, T. (1981). *J. Phys.* B **14**, L255.

Appendix. ECPSSR Theoretical Calculations

Following the method of Brandt and Lapicki (1979, 1981) the equation for the ECPSSR theoretical cross section is

$$\sigma_s^{\mathrm{ECPSSR}} = C\big(2dq_{0s}\zeta_s/(z_s^2+z_s)\big)(\sigma_{0s}/\zeta_s\theta_s)F_s\big(m_s^{\mathrm{R}}(\xi_s/\zeta_s)\eta_s/(\zeta_s\theta_s)^2, \zeta_s\theta_s\big), \tag{A1}$$

where the subscript s refers to the target subshell. The parameters in the above equation are defined as follows:

$$C(x) = vE_{v+1}(x) \tag{A2}$$

is the Coulomb deflection factor where $E_n(x)$ is the exponential integral of order n ($v = 9$ for the K and L_1 shells and $v = 11$ for the L_2 and L_3 shells);

$$d = Z_1 Z_2/Mv_1^2 \tag{A3}$$

is the half-distance of closest approach in a head-on collision and where $M = M_1 M_2/(M_1+M_2)$;

$$q_{0s} = U_{2s}/v_1 \tag{A4}$$

is the minimum momentum transfer (atomic units) for $\Delta E \ll E_1$ and small ejected electron kinetic energy ε_f, where ΔE is the energy transfer equal to $U_{2s}+\varepsilon_f$, and U_{2s} is the observed binding energy (the subscripts 1 and 2 refer to the projectile and target respectively);

$$\zeta_s = 1+(2Z_1/Z_{2s}\theta_s)(g_s-h_s), \tag{A5}$$

where g_s and h_s are tabulated analytical functions (see Basbas *et al.* 1978; Brandt and Lapicki 1979) of the reduced ion velocity ξ_s representing changes in the binding parameter θ_s due to increased binding (close collisions) and polarization of the target state (distant collisions) respectively;

$$z_s = \{1-4(\zeta_s/\xi_s)^2/M\zeta_s\theta_s\}^{\frac{1}{2}} \tag{A6}$$

represents the energy loss of the ion in traversing the target atom system (and hence appears only in the argument for the Coulomb deflection factor for exact limits of integration);

$$\sigma_{0s} = (2j+1)4\pi a_{2s}^2(Z_1/Z_{2s})^2 \tag{A7}$$

may be viewed as a wave mechanical cross section $4\pi a_{2s}^2$ ($a_{2s} = n^2/Z_{2s}$ is the average target s-shell radius, with principal quantum number n, in atomic units) for each of the $2j+1$ electrons, weighted by the square of the Coulomb interaction strength;

$$F_s(x,y) = 2f_s(x,y)/(2j+1)n^4xy \tag{A8}$$

is the so-called reduced universal cross section and is a function of the reduced projectile energy η_s and reduced binding energy θ_s corrected for Coulomb deflection, binding and relativistic effects (while m^{R} is the 'local' relativistic electron mass as defined by Brandt and Lapicki 1979).

Also, in equation (A8) we have

$$f_s(x,y) = \int_{W_{\min}}^{W_{\max}} \mathrm{d}W \int_{Q_{\min}}^{Q_{\max}} \mathrm{d}Q\, |F_{W,s}(Q)|^2/Q^2\,, \tag{A9}$$

where (using atomic units)

$$W = 2\Delta E/Z_{2s}^2 \tag{A10}$$

(ΔE is the energy transfer to the atom in the centre-of-mass frame) and

$$Q = q^2/Z_{2s}^2 \tag{A11}$$

(q is the momentum transfer); $F_{W,s}(Q)$ is the form factor for the transition between the initial and final target electron states and can be expressed algebraically in terms of Q and W (see e.g. Benka and Kropf 1978);

$$Q_{\min} = (q_0/Z_{2s})^2 \tag{A12}$$

and

$$q_0 = (2ME/m)^{\frac{1}{2}}\{1-(1-\Delta E/E)^{\frac{1}{2}}\}\,, \tag{A13}$$

hence

$$Q_{\min} = (2ME/Z_{2s}^2 m)\{1-(1-\Delta E/E)^{\frac{1}{2}}\}^2\,, \tag{A14}$$

where E is the centre-of-mass energy of the system ($=ME_1/M_1$) and m is the electron mass (equal to 1 in atomic units). From the expressions for the reduced projectile energy,

$$\eta_s = 2E_1 m/M_1 Z_{2s}^2\,, \tag{A15}$$

and for W (equation A10), we have in equation (A14)

$$2ME/Z_{2s}^2 m = \eta_s(M/m)^2\,, \qquad \Delta E/E = Wm/\eta_s M\,,$$

hence

$$Q_{\min} = \eta_s(M/m)^2\{1-(1-Wm/\eta_s M)^{\frac{1}{2}}\}^2\,, \tag{A16}$$

$$Q_{\max} = \eta_s(M/m)^2\{1+(1-Wm/\eta_s M)^{\frac{1}{2}}\}^2\,. \tag{A17}$$

The minimum energy transfer (for ionization) to the target atom is just the observed binding energy U_{2s} and the maximum energy transfer is simply E; hence

$$W_{\min} = 2U_{2s}/Z_{2s}^2 = \theta_s/n^2 \tag{A18}$$

in terms of the reduced binding parameter, and

$$W_{\max} = 2E/Z_{2s}^2 = \eta_s(M/m) \tag{A19}$$

in terms of the reduced energy parameter.

Manuscript received 30 March, accepted 2 July 1984